Photoluminescence properties of CaWO4 and CdWO4 thin films deposited on SiO2/Si substrates

Aziz Taoufyq, Valerie Mauroy, Tomas Fiorido, Frédéric Guinneton, Jean-Christophe Valmalette, Bahcine Bakiz, Abdeljalil Benlhachemi, Abdallah Lyoussi, Gilles Nolibe, Jean-Raymond Gavarri

Version of Record: https://www.sciencedirect.com/science/article/pii/S0022231319308191
Manuscript_67b909e1031258cbed58d84c3892c095

Photoluminescence properties of $CaWO_4$ and $CdWO_4$ thin films deposited on SiO_2/Si substrates

Aziz Taoufyq[a], Valerie Mauroy[b], Tomas Fiorido[c], Frédéric Guinneton[b], Jean-Christophe Valmalette[b], Bahcine Bakiz[a], Abdeljalil Benlhachemi[a], Abdallah Lyoussi[d], Gilles Nolibé[e], Jean-Raymond Gavarri[b,*]

[a] *Laboratory Materials and Environment (LME), Faculty of Sciences, University Ibn Zohr, B.P 8106, City Dakhla, Agadir, Morocco.*

[b] *University of Toulon, Aix-Marseille University, CNRS 7334, IM2NP, 83957 La Garde Cedex, France*

[c] *Aix-Marseille University, University of Toulon, CNRS 7334, IM2NP, 13397 Marseille Cedex 20, France*
d The CEA of Cadarache, DEN, Department of reactors studies, experimental physics, Instrumentation Sensors and Dosimetry Laboratory, 13108 Saint-Paul Lez Durance, France

[e] *CESIGMA Signals & Systems, 83220 Le Pradet, France*

(*) To whom correspondence must be addressed: gavarri.jr@univ-tln.fr & gavarri.jr@gmail.com

ABSTRACT

In this study, we present photoluminescence (PL) analyses under UV and X-ray excitations of thin layers of $CaWO_4$ and $CdWO_4$ deposited on SiO_2/Si substrates, by radio-frequency sputtering method. The main objective was to determine the efficiency of PL emissions in the case of these specific SiO_2/Si substrates. Polycrystalline $CaWO_4$ and $CdWO_4$ phases were used as standards for PL emission analyses. Characterizations of films were carried out by X-ray diffraction, scanning electron microscopy, and atomic force microscopy. The PL experiments were carried out under monochromatic UV and polychromatic X-ray excitations. The PL intensities varied with tungstate film thicknesses. In the case of X-ray excitation, oscillations of PL intensities were observed. These oscillations corresponded to interferences of PL emissions, strongly correlated with the thickness of intermediate SiO_2 layers. A Fabry-Perot model simulating these oscillations is applied allowing differentiating the PL responses of these films.

Keywords: $CaWO_4$, $CdWO_4$, thin films, photoluminescence, oscillations, interferences

1. Introduction

By the past, materials AXO_4 (X=W, Mo) based on tungstate or molybdate anions have been extensively studied to develop diversified applications. These compounds are susceptible to be integrated into new radiation sensors, in order to be used in different fields of applications such as reactor measurements, safeguards, homeland security, nuclear nondestructive assays, LINAC emission radiation measurement [1- 4]. The systems based on calcium or cadmium tungstate ($CaWO_4$ or $CdWO_4$) were previously investigated for their potential applications in many fields such as photoluminescence [5-11], microwave applications [12- 14], optical fiber scintillator material [15, 16], humidity sensors and catalysis [17, 18]. These two tungstate phases were previously synthesized by coprecipitation method [19, 20], solid-state reaction [21, 22], sol-gel method [23, 24] and hydro/solvo-thermal method [25- 29]. The $CaWO_4$ and $CdWO_4$ structures belong respectively to the scheelite [12, 23] (tetragonal) and wolframite [29, 30] (monoclinic) systems. In our previous studies [19, 20], the photoluminescence of $Ca_{1-x}Cd_xWO_4$ polycrystalline solid solution was studied under UV and X-ray excitations. Now, our objective is to develop photoluminescent thin layers of $CaWO_4$ and $CdWO_4$, to be integrated into miniaturized devices for sensing applications. In the present work, we optimize the deposition process of thin films of $CaWO_4$ and $CdWO_4$ on SiO_2/Si substrates and characterize their photoluminescence under UV and X-ray excitations. Photoluminescence oscillations are observed and interpreted.

2. Experimental methods

2.1. Syntheses

The detailed method of preparation of polycrystalline standards can be found in a previous publication [19, 20]. The preliminary precursors were calcium and cadmium nitrate and sodium tungstate in aqueous solutions. Finally, the solid precursors obtained by coprecipitation were heated under air, at 1000 °C for 3 hours. Thin films of calcium and cadmium tungstates, using these $CaWO_4$ and $CdWO_4$ polycrystalline precursors in forms of pellets, were deposited at room temperature, by radio-frequency sputtering method, on commercial SiO_2/Si substrates (supplied by IBS Society, with SiO_2 thicknesses of 2000 ± 100 nm). X-ray diffraction preliminary analyses showed that all as-deposited thin films were amorphous. After thermal heating at 600 °C, in an air atmosphere, crystalline phases of

$CaWO_4$ and $CdWO_4$ were obtained. **Table 1** gives the deposition parameters for three types of thin films with three characteristic thicknesses.

2.2. Profilometry analysis

To determine the thickness of thin films, a Dektak 6M, Stylus Profiler of VEECO society was used. The three types of film thicknesses are indicated in Table 1.

Table 1: Deposition parameters of radio-frequency sputtering device

2.3. X-ray diffraction (XRD)

Using an Empyrean - Panalytical diffractometer equipped with copper source and Ni filter, the polycrystalline samples were analyzed in classical θ–2θ configuration, while the thin films were analyzed in specific grazing incidence. A detailed structural determination from Rietveld method was performed to characterize the standards $CaWO_4$ and $CdWO_4$ [19]. The XRD analyses of thin films were carried out in grazing incidence with an optimized incidence angle of 3 deg. 2θ. The patterns were registered in the angular range 10 to 80 deg. 2θ with a step of 0.00164 deg. and a rotation speed of 0.002 $deg.s^{-1}$.

2.4.Scanning electron microscopy (SEM)

Surface images of $CaWO_4$ and $CdWO_4$ films were obtained from Zeiss-Supra 40 VP/Gemini Column scanning electron microscope (SEM). These images coupled to Energy Dispersive X-rays Spectroscopy (EDXS) allowed analyzing the various morphologies and local compositions of samples.

2.5.Atomic force microscopy (AFM)

A microscope AFM XE-100 from PSIA was used to observe the thin films surfaces at a nanoscale. Roughness of films was determined.

2.6.Photoluminescence (PL) analyses

The experimental X-ray source used to irradiate the samples was the previously described X-ray diffraction equipment equipped with a copper source. The nominal emission conditions (voltage V_{RX} / current I_{RX}) were 45 kV/35 mA. The resulting excitation energies ranged between 0 and 45 keV, with a maximum located at about 20 keV. It should be noted that the X-ray source also delivered the classical transition energies of copper source. The polycrystalline samples were in form of 2 mm thick cylindrical pellets (13 mm diameter), compacted under a pressure of 5 kbars. The surfaces were placed at a constant distance of the

X-ray source, of about 10 cm, set with a fixed inclination relative to the incident X-ray beam. The photoluminescence emissions of samples were recorded using a UV – visible spectrophotometer MicroHR (Jobin Yvon) equipped with an optical fiber of 400 μm in diameter. The fiber was set at a fixed distance of the sample surfaces (1 mm), perpendicularly to the sample surface. The constant dimensions of the irradiated grain rectangular surfaces were of about 2 mm/20 mm.

The UV excitations were obtained from a spectrometer Horiba Jobin Yvon model LabRam HR800 allowing Raman spectroscopy or photoluminescence analyses. The laser excitation was obtained from ionized argon laser with energy of 3.40 eV or wavelength 364.5 nm, and delivering a power on surface samples of 5 μW.

For thin films, all photoluminescence experiments were carried out in the same irradiation conditions (incident energies, irradiated surface) to allow comparing their PL responses.

3. Results and discussion

3.1. Polycrystalline targets

The detailed structures of polycrystalline samples of $CaWO_4$ and $CdWO_4$ were analyzed in a previous work [19, 20] using Rietveld method. Figures 1a and 1b report the calculated and observed diffraction patterns for polycrystalline $CaWO_4$ and $CdWO_4$ thermally treated at 1000 °C, showing a good crystallization and absence of any significant residual phase.

Fig. 1a. Experimental and calculated diffraction profiles of $CaWO_4$ (Rietveld analysis, see [19, 20]), thermally treated at 1000 °C for 3 h.

Fig. 1b. Experimental and calculated diffraction profiles of $CdWO_4$ (Rietveld analysis, see [19,20]), thermally treated at 1000 °C for 3 h.

3.2.Thin films

Three types of thin films deposited on SiO_2/Si substrates were selected and their thicknesses were determined by profilometry technique: $CdWO_4$ thin films having 200 and 400 nm of thicknesses, $CaWO_4$ thin film having 600 nm of thickness. Figures 2a and 2b report the X-ray diffraction patterns (from grazing incidence configuration) of typical $CaWO_4$ and $CdWO_4$ thin films, respectively 600 nm and 400 nm thick, deposited on 2 μm thick SiO_2 layer on Si substrate. The initial SiO_2 patterns are shown. Having regard to the low quality of such X-ray diffraction records directly linked to the grazing incidence configuration, the determination of

approximate cell parameters was carried out to clearly identify the phases and residues. **Table 2** gives the different results.

Fig. 2a. X-ray diffraction patterns of $CaWO_4$ (600 nm) thin films (up), SiO_2/Si substrate before deposition and standard profile from JCPDS file 00-041-1431 (down).

Fig. 2b. X-ray diffraction patterns of $CdWO_4$ (400 nm) thin films (up), SiO_2/Si substrate before deposition and standard profile from JCPDS file 00-041-0676 (down).

Table 2: Refined cell parameters of $CdWO_4$ (monoclinic wolframite) and $CaWO_4$ (tetragonal scheelite) phases formed in thin films after thermal treatment at 600 °C.

3.3. Analyses of thin films surfaces

The SEM images of **Figures 3a and 3b** show the surfaces of $CaWO_4$ (600 nm thickness) and $CdWO_4$ (400 nm thickness) respectively.

Fig. 3a. SEM images of $CaWO_4$ film (600 nm) surface. Crystallites (45 nm) and cracks are observed. Chemical composition Ca/W from EDX close to 1 (±0.1)

Fig. 3b. SEM images of $CdWO_4$ film (400 nm) surface. Crystallites (50 nm) and cracks are observed. Chemical composition Cd/W from EDX close to 1 (±0.1)

Average sizes of crystallites were statistically determined: they were of 50 nm in $CaWO_4$ film and 45 nm in $CdWO_4$ film. The surface morphologies were characteristic of the formation of interconnected crystallites perpendicular to the film surface, with presence of cracks due to surface stresses.

3.3.AFM analyses of surfaces

Figures 4a, b, c, d, e and 5a, b, c, d, e report AFM images of $CdWO_4$ (400 nm) and $CaWO_4$ (600 nm) thin films with their 3D representations. These AFM analyses showed significant variation in the surface morphologies of the two films of $CdWO_4$ (400 nm) and $CaWO_4$ (600 nm). The average roughness R_q measured on an area of 1 μm x 1μm is of the order of 11 nm for $CdWO_4$ thin film and 4 nm for $CaWO_4$ thin film.

Fig. 4a, b, c, d, e. AFM analysis with 3D representation of $CaWO_4$ thin layer. (a) and (b) (5x5 μm^2 surface); (c) and (d) (1x1 μm^2 surface); (e) AFM profile for roughness determination (Z in nm).

Fig. 5a, b, c, d, e. AFM analysis with 3D representation of $CdWO_4$ thin layer. (a) and (b) (5x5 μm^2 surface); (c) and (d) (1x1 μm^2 surface); (e) AFM profile for roughness determination (Z in nm).

3.4.Photoluminescence analyses of polycrystalline phases

The polycrystalline $CaWO_4$ and $CdWO_4$ phases compacted in forms of cylindrical pellets were subjected to irradiations under UV and X-ray excitations.

Figures 6a and 6b report the typical PL emission profile of polycrystalline $CaWO_4$ and $CdWO_4$ obtained under UV excitation (364 nm, 3.4 eV). For $CdWO_4$, the maximum of PL band is located at 575 nm or 2.15 eV. A quite similar profile was obtained for the $CaWO_4$ sample with a band located at 610 nm or 2.05 eV.

Figures 6c and 6d show the PL bands of $CaWO_4$ (2.62 eV) and $CdWO_4$ (2.40 eV) obtained under X-ray excitation. Each band was decomposed in several gaussian components corresponding to charge transfers in WO_4 and WO_6 groups. The differences in energies can be ascribed to the tetrahedral and octahedral configurations WO_4 and WO_6 in scheelite and wolframite structures.

Figure 7 recall the two classical schematic energy levels diagrams relative to the WO_4^{2-} and WO_6^{6-} groups present in the two different $CaWO_4$ and $CdWO_4$ structures, respectively. In $CaWO_4$ two main transitions $^3T_1$, $^3T_2$ ➔ $^1A_1$ are expected. In $CdWO_4$ two main transitions $^3T_{1u}$, $^3T_{1u}$ ➔ $^1A_1$ and two spin forbidden transitions $^1T_{1g}$, $^3T_{1g}$ ➔ $^1A_1$ (possibly observed through spin orbit coupling) are expected. Due to vacancies and Jahn Teller effects these transitions can be modified, and additional components can be observed.

Fig. 6a, b. PL band observed in $CaWO_4$ and $CdWO_4$ polycrystalline samples exposed to monochromatic UV excitation (364.5 nm).

Fig. 6c, d. (a) PL band of $CaWO_4$ (scheelite) exposed to polychromatic X-ray excitation and decomposition into four gaussian components; (b) PL band of $CdWO_4$ (wolframite) and decomposition into three gaussian components.

Fig. 7. Schematic energy levels diagrams associated with the photoluminescence of scheelite $CaWO_4$ (on the left) and wolframite $CdWO_4$ (on the right) phases, according to [33].

All literature references can be found in our previous works. These PL emissions are generally attributed to specific allowed electronic transitions between W* antibonding levels

and oxygen O2p bonding levels, characteristic of tungstate groups [31-34]. The variations of emission intensities was ascribed to the existence of several types of defects resulting from elaboration conditions: (i) presence of WO_3 clusters among the WO_4 expected clusters, (ii) presence of oxygen vacancies (noted as V_O) in WO_4 clusters described as $[WO_3V_O]$ clusters, presence of cation (Ca and Cd) vacancies, all defects resulting from elaboration processes. In the case of scheelite structures the emissions would be strongly linked to charge transfer in WO_4^{2-} oxyanions, while in the case of wolframite structures the emissions would be associated with charge transfers in WO_6^{6-} oxyanions.

3.6. Photoluminescence of thin films

The photoluminescence of thin layers of $CaWO_4$ and $CdWO_4$ was studied under UV and X-ray excitations. Due to the small amount of matter on thin films, the PL signals were recorded during exposition time of 2 hours for each film (under X-ray excitations). **Figures 8 a and 8 b** compare the different spectra obtained from thin film $CaWO_4$ (400 nm) and $CdWO_4$ (400 nm) under UV (on the left) and X-Ray (on the right) excitations. In the case of UV excitation (left figure), we observe two continuous spectra similar to the luminescence spectra of polycrystalline samples $CaWO_4$ and $CdWO_4$, with a very weak signal for $CaWO_4$. In the case of X-ray excitation, oscillations are observed for $CaWO_4$ and $CdWO_4$ layers. The different profiles of PL emissions were previously ascribed to the low and high UV and X-ray beams penetration in the materials.

Fig. 8a, b. Luminescence of $CdWO_4$ and $CaWO_4$ thin layers (thicknesses of 400 nm): (a) under UV excitation (left figure); (b) under X-ray excitation (right figure).

In **Figure 9**, we have reported various PL spectra obtained under X-ray excitation with $CaWO_4$ (600 nm), $CdWO_4$ (200 nm) and $CdWO_4$ (400 nm) thin films. The separations between maxima of intensities are respectively of $\Delta E(CdWO_4\text{-}200nm) = 0.15$ eV, $\Delta E(CdWO_4\text{-}400nm) = 0.17$ eV and $\Delta E(CaWO_4\text{-}600\ nm) = 0.18$ eV.

Fig. 9. Oscillations observed for $CdWO_4$ (400 nm, strongest signal), $CdWO_4$ (200nm, intermediate signal), $CaWO_4$ (600 nm, weak signal). The centroids are 2.5 eV for $CdWO_4$ thin films and 2.65 eV for $CaWO_4$.

In the case of $CaWO_4$ films (400 nm), the PL band observed under X-ray excitation (Fig. 9) was centered at 2.7 eV, very weak in intensity and with poor statistical definition. In the case of $CdWO_4$ films, a clear PL spectrum was observed under X-ray excitation (Fig. 9), centered at 2.5 eV.

These interferences can be interpreted from the Fabry-Perot model [35, 36] applied to thin layers. These oscillations in emission spectra were directly interpreted by authors *Huang et al*. [36] in terms of optical interferences linked to the thin layer thickness L. They depend on the quality of interfaces film/substrate and are due to the presence of cavities perpendicular to the films.

The optical transmittance Tr in the case of two parallel interfaces can be expressed in a simplified form, with $\Delta\Phi = 2nLk.\cos\theta$ being the phase difference, where 2nL is the elemental optical path, θ the incidence angle, $k = 2\pi/\lambda$, R the reflectivity coefficient. Then, a classical calculation gives:

$$Tr(\lambda) = 1 / [\, 1 + (4R/(1-R)^2).(\sin(\Delta\Phi/2))^2]$$

This expression allows calculating the associated reflectance $Ref(\lambda) = 1 - Tr(\lambda)$ assuming that absorbance could be neglected.

From this expression, we can calculate the separation of angle phases between two maxima of this function $Ref(\lambda)$:

$$\delta\Delta\Phi/2 = n.L.\cos\theta.2\pi\,[1/\lambda_1 - 1/\lambda_2] = \pi \Rightarrow 2nL\cos\theta\,(\Delta\lambda / (\lambda_1.\lambda_2) = 1$$

Considering $\lambda_1.\lambda_2 = \langle\lambda\rangle^2$, we obtain the resulting relation: $2nL\cos\theta = \langle\lambda\rangle^2 / \Delta\lambda = hc/\Delta E$ where ΔE is the energy separation between two maxima.

It should be noted that, in the present configuration, the angle $\theta = 0$ (fiber perpendicular to the film surfaces). From this formula, if the n value could be assumed to be quasi constant and close to 1.5 (approximate n value for SiO_2), and having regard to the small variation of ΔE as L increases in our experiments, the calculated dimensions L would be close to 3000 nm, higher than the observed thin layer thicknesses (200, 400, 600 nm). This could be due to the presence of the 2 μm thick intermediate SiO_2 layer separating the deposited films and Si substrate. The oscillations clearly evidenced in the case of X-ray excitations would be due to Fabry-Perot interferences provoked by the SiO_2 layer formed on the Si substrate. The PL emission of the thin layers would be due to excitation by X-ray beam penetrating the thin layers: at the interface layer / SiO_2 the X-ray emission could be guided by specific columns with index n of refraction and the reflection on the interface SiO_2/Si could emerge and

interferences would occur. As the interfaces are irregular, the optical path would be composed of a distribution of optical lengths nL with variable n and L values. The L values would correspond only to the thicknesses of the SiO_2 layers on Si substrate and would be known with only 5 % of error.

The oscillations observed in our experiments could result from two types of effects:

(a) Variable nL optical lengths,

(b) or superposition of a direct PL emission from the thin film surfaces and interferences due to emission circulating through SiO_2 and being reflected by SiO_2/Si interfaces.

Assuming L values of SiO_2 layer close to 2000 nm, we have tested both hypotheses.

The general expression used to simulate the observed signals (PL emission with oscillations) was:

$$I(\lambda) = X.\, I_{st}(\lambda).\, Refl(\lambda) + (1 - X).\, I_{st}(\lambda)$$

where the $I_{st}(\lambda)$ function should be a standard emission profile (from polycrystalline sample) under the form of experimental data or gaussian functions obtained from the emission profiles of polycrystalline samples.

A typical simulation is reported in Figure 10. It makes use of a standard experimental profile $I_{st}(\lambda)$ (see PL emission of $CdWO_4$ above, Fig. 7 b), and a theoretical function (in arbitrary units) $Refl(\lambda)$. The optimized resulting profile (experimental multiplied by theoretical) is obtained with four variable nL values (nL = 4000, 3800, 3500, 3300), R = 0.6 and X = 1 (unique system). These four adapted nL values should correspond to four n values of 2, 1.9, 1.75 and 1.65 greater than the value of 1.5 expected for SiO_2. Other simulations with X<1 and only one nL value did not deliver any satisfactory optimization.

Fig. 10. Calculated oscillating profile of PL emission obtained under X-ray excitation (45 kV/35 mA) from a system $CdWO_4$ film/SiO_2/Si with nL variable (4000, 3800, 3500, 3300) R=0.6. $<\Delta E>$ value = 0.17 eV. Black squares: experimental emission profile for a standard $CdWO_4$ polycrystalline material. Black points: calculated profile in arbitrary units.

This simulation was obtained with nL values delivering effective average n values of about 1.75 (not 1.5, the expected value of n for SiO_2). This could characterize a strong inhomogeneity in the materials. Having regard to the experimental errors on L values (mainly

SiO_2 thicknesses) of about 5 %, the ΔE variations (of about 0.03 eV) observed in our experiments might be linked to variations of Δn/n = 15 % where Δn is a variation of average n value, n being an average value. In other terms, the variation of average n value would be of 0.3 for an average n value of 1.75.

4. Conclusions

In these studies, thin films of $CdWO_4$ and $CaWO_4$ have been deposited on SiO_2/Si substrates and photoluminescence spectra recorded under UV and X-ray irradiations were analyzed. The photoluminescence of thin layers is characterized by the presence of oscillations of intensities, mainly observable under X-ray excitation, even if they might be weakly suggested by smooth undulations in the case of UV excitation. These observations have been interpreted in terms of interferences related to the SiO_2 intermediate layer. The classical Fabry-Perot model has been used to simulate such oscillations, showing that this feature cannot be ascribed to the sole thicknesses of $CaWO_4$ or $CdWO_4$ deposited on the intermediate SiO_2 layer. As L values are given with errors of less than 5%, the variations of optical path n.L are mainly due to the modification of optical refraction index n. In other terms, the determinations of ΔE could be used to evaluate the variations of refraction optical index n in such thin films, variations resulting from material inhomogeneity and probably from the various interfaces (film/SiO_2/Si).

Acknowledgements

This work was financially supported by the Regional Council of Provence-Alpes - Côte d'Azur, the European Funds for Regional Development, the General Council of Var and by Toulon Provence Mediterranean, in the general framework of NANOGAMMA project (Grant number: 2010-16028/42169) and ARCUS-CERES international project. It results from a collaboration between IM2NP, CEA of Cadarache, CESIGMA and IBS Societies.

References

[1] H. Amharrak, J. Di Salvo, A. Lyoussi, A. Roche, M. Masson-Fauchier, J.C. Bosq, M. Carette, IEEE Trans. Nucl. Sci. 59 (4) (2011) 1360-1368.

[2] D. Fourmentel, C. Reynard-Carette, A. Lyoussi, J-F. Villard, J-Y. Malo, M. Carette, J. Brun, P. Guimbal, Y. Zerega, IEEE Trans. Nucl. Sci. 60 (1) (2013) 328-335.

[3] A. Lyoussi, J. Romeyer-Dherbey, F. Jallu, E. Payan, A. Buisson, G. Nurdin, J. Allano, J. Nucl. Instr. Meth. Phys. Res. B. 160 (2) (2000) 280-289.

[4] A. Sari, F. Carrel, M. Gmar, F. Laine, A. Lyoussi, S. Normand, IEEE Trans. Nucl. Sci. 59 (3) (2012) 605-611.

[5] L. Gracia, Valéria M. Longo, Laécio S. Cavalcante, A. Beltrán, W. Avansi, M. S. Li, V. R. Mastelaro, J. A. Varela, E. Longo and J. Andrés, J. Appl. Phys. 110 (4) (2011) 043501.

[6] H.F. Hameka, C.C. Vlam, Physica, 19 (1953) 943-949.

[7] T. Thongtem, S. Kungwankunakorn, B. Kuntalue, A. Phuruangrat, S. Thongtem, J. Alloys Comp. 506 (2010) 475-481.

[8] D. Spassky, V. Mikhailin , M. Nazarov , M.N. Ahmad-Fauzi, A. Zhbanov, J. Lumin. 132 (2012) 2753-2762.

[9] V.B. Mikhailik, H. Kraus, D. Wahl, M. Itoh, M. Koike, I. K. Bailiff , J. Phys. Rev. B, 69 (20) (2004) 205110-205110-9.

[10] R. Grasser, A. Scharmann, J. Lumin. 12-13 (1976) 473-478.

[11] W. Zhang, J. Long , A. Fan , J. Li, J. Mat. Res. Bull. 47 (2012) 3479-3483.

[12] J.C. Sczancoski, L.S. Cavalcante,M.R. Joya, J.A. Varela, P.S. Pizani, E. Longo, J. Chem. Eng. 140 (2008) 632-637.

[13] T. Thongtem, A. Phuruangrat and S. Thongtem, J. Mat. Lett. 62 (2008) 454-457.

[14] J. Liu, J. Ma, B. Lin , Y. Ren , X. Jiang , J. Tao , X. Zhu, Ceram. Int. 34 (2008) 1557-1560.

[15] M. Nikl, P. Bohacek, E. Mihokova, N. Solovieva, A. Vedda, M. Martini, G.P. Pazzi, P. Fabeni, M. Kobayashi, and M. Kobayashi, J. Appl. Phys. 91(8) (2002) 5041-5044.

[16] M.Nikl, P.Bohacek, E.Mihokova, M.Kobayashi, M.Ishii, Y.Usuki, V.Babin, A.Stolovich, S.Zazubovich, M.Bacci, J. Lumin. 87-89 (2000) 1136-1139.

[17] T. Thongtem, A. Phuruangrat and S. Thongtem, J. Ceram. Process. Res. 9 (3) (2008) 258-261.

[18] C.S. Lim, K.H. Kim and K.B. Shim, J. Ceram. Process. Res.12 (6) (2011) 727-731.

[19] A.Taoufyq, F. Guinneton, J-C. Valmalette, M. Arab, A. Benlhachemi, B. Bakiz, S. Villain, A. Lyoussi, G. Nolibe, J-R. Gavarri, J. of Sol. St. Chem. 219 (2014) 127-137.

[20] A.Taoufyq, V. Mauroy, F. Guinneton, B. Bakiz, S. Villain, A. Hallaoui, A. Benlhachemi, G. Nolibe, A. Lyoussi, J-R. Gavarri, Journal of Materials Research Bulletin, 70 (2015) 40-46.

[21] Luke L. Y. Chang, G. Margaret Scroger, B. Phillips, J. Am. Ceram. Soc. 49 (7) (1966) 385-390.

[22] Luke L. Y. Chang, The Amer. Mineral. 52 (1967) 427-435.

[23] A. Katelnikovas , L. Grigorjeva , D. Millers , V. Pankratov , and A. Kareiv, Lith. J. Phys. 47 (1) (2007) 63-68.

[24] K. Lennstrom, S.J. Limmer, G. Cao, J. Thin Solid Films, 434 (2003) 55.

[25] Y. Ling, L. Zhou, L. Tan, Y.Wang, C. Yu, J. Cryst. Eng. Comm. 12 (2010) 3019-3026.

[26] W.S. Wang, L. Zhen, C.Y Xu, Li Yang, and W.Z. Shao, J. Phys. Chem. C 112 (2008) 19390-19398.

[27] A. J. Rondinone, M. Pawel, D. Travaglini, S. Mahurin, S. Dai, J. Colloid Interface. Sci. 306 (2) (2007) 281-285

[28] Tingjiang Yan, Liping Li,Wenming Tong, Jing Zheng,YunjianWang, Guang she Li, J. Solid state. Chem. 184 (2011) 357-364 .

[29] L. S. Cavalcante, V. M. Longo, J. C. Sczancoski, M. A. P. Almeida, A. A. Batista, J. A. Varela, M. O. Orlandi, E. Longoa, M. Siu Li, J. Cryst. Eng. Comm. 14 (2012) 853-868.

[30] Chang Sung Lim, J. Mat. Chem. Phys. 131 (2012) 714-718.

[31] S.L. Pôrto , E. Longo , P.S. Pizani, T.M. Boschi, L.G.P. Simôes, S.J.G. Lima , J.M. Ferreira, L.E.B. Soledade , J.W.M. Espinoza , M.R. Cassia-Santos , M.A.M.A. Maurera , C.A. Paskocimas , I.M.G. Santos, A.G. Souza, J. Solid state . Chem. 181 (2008) 1876-1881.

[32] E. Orhan, , M. Anicete-Santos, M.A. Maurera, M.F. Pontes, A.G. Souza, J. Andres, A. Beltran, J.A. Varela, P.S. Pizani, C.A. Taft, E. Longo, J. Solid state. Chem.178 (2005) 1284-1291.

[33] V.B. Mikhailik, H. Kraus, G. Miller, M.S. Mykhaylyk, D. Wahl, J. Appl. Phys. 97 (2005) 083523- 083523-8.

[34] M. Bacci, S. Porcinai, E. Mihokova, M. Nikl, and K. Polak, Phys. Rev. B. 64 (2001) 104302.

[35] M. I. Nathan, A. B. Fowler, and G. Burns, Phys. Rev. Lett. 11, 152 (1963).

[36] K. Huang, L. Pu, Y. Shi, P. Han, R. Zhang, and Y. D. Zheng, J. Appl. Phys. Lett., 89 (2006) 201118.

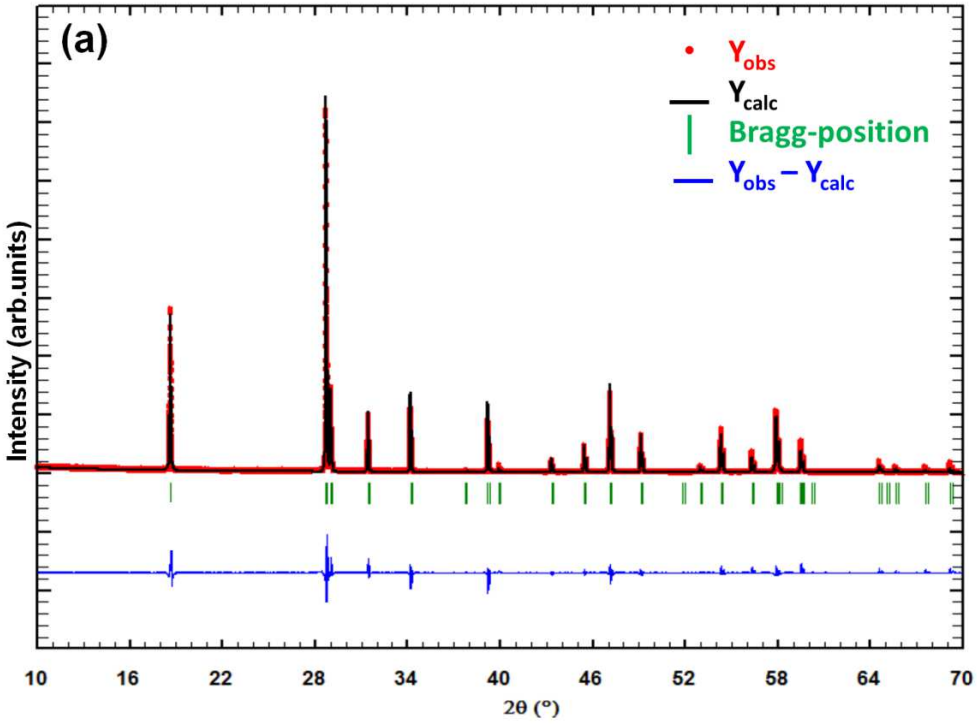
(a)
Y_obs
Y_calc
Bragg-position
Y_obs – Y_calc
Intensity (arb.units)
10
16
22
28
34
40
46
52
58
64
70
2θ (°)

Fig. 1a

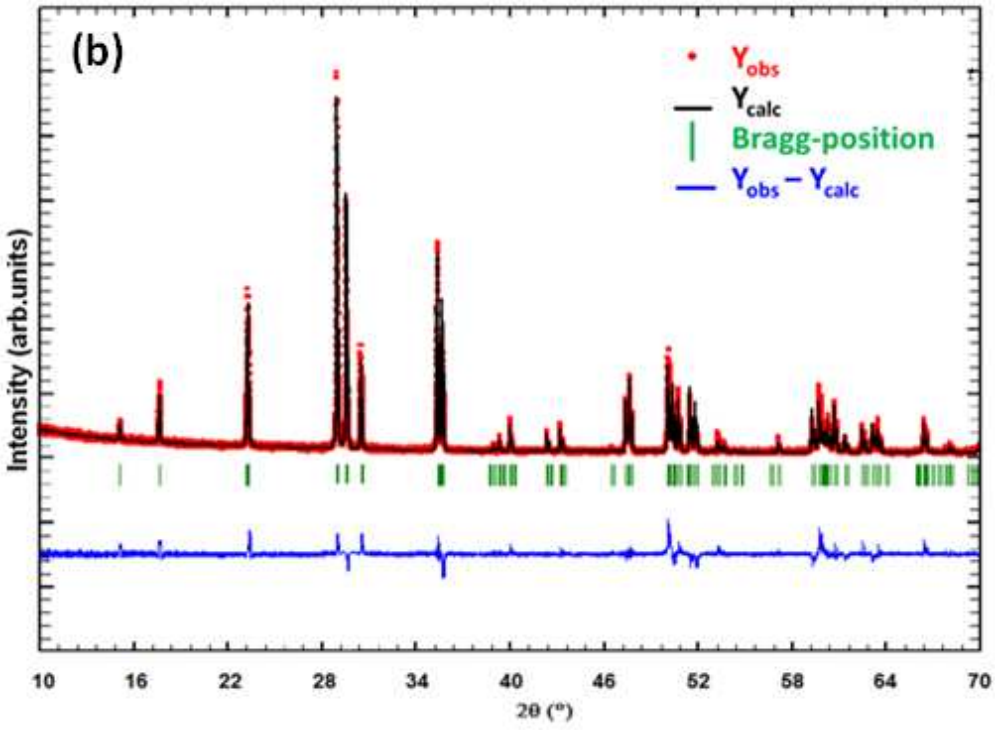
(b)
Y_obs
Y_calc
Bragg-position
Y_obs – Y_calc
Intensity (arb.units)
10
16
22
28
34
40
46
52
58
64
70
2θ (°)

Fig. 1b:

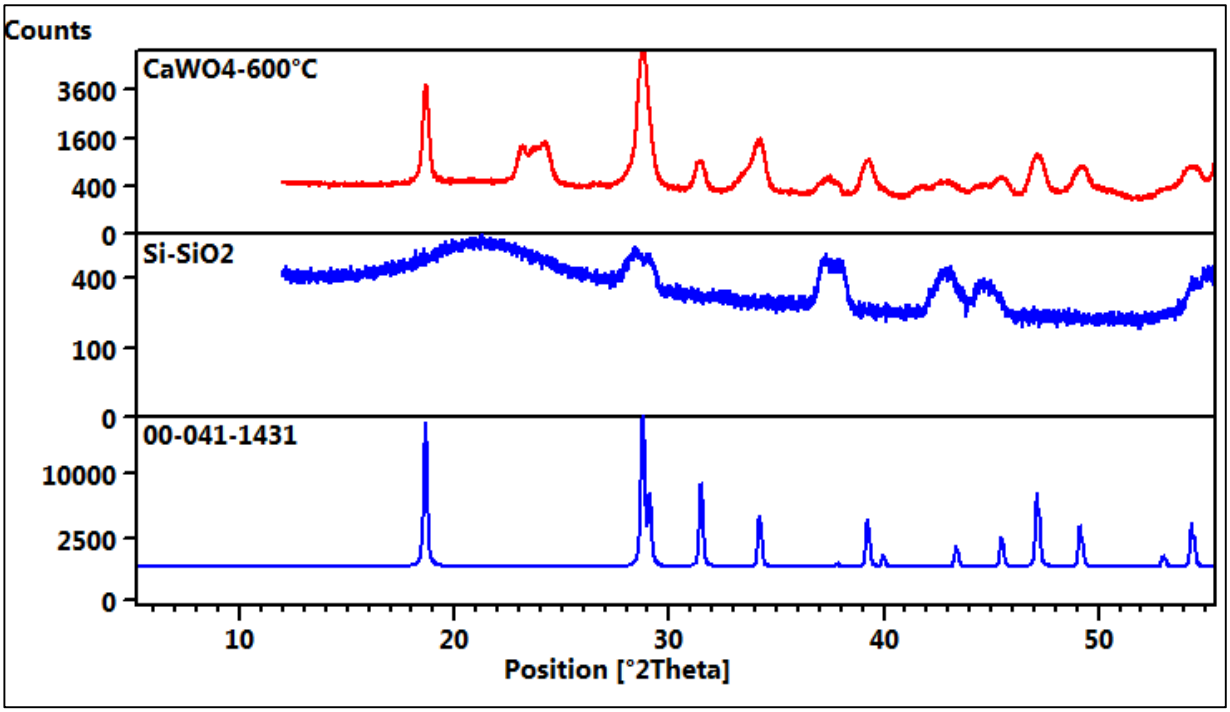
Counts
CaWO4-600°C
3600
1600
400
0
Si-SiO2
400
100
0
00-041-1431
10000
2500
0
10
20
30
40
50
Position [°2Theta]

Fig. 2a:

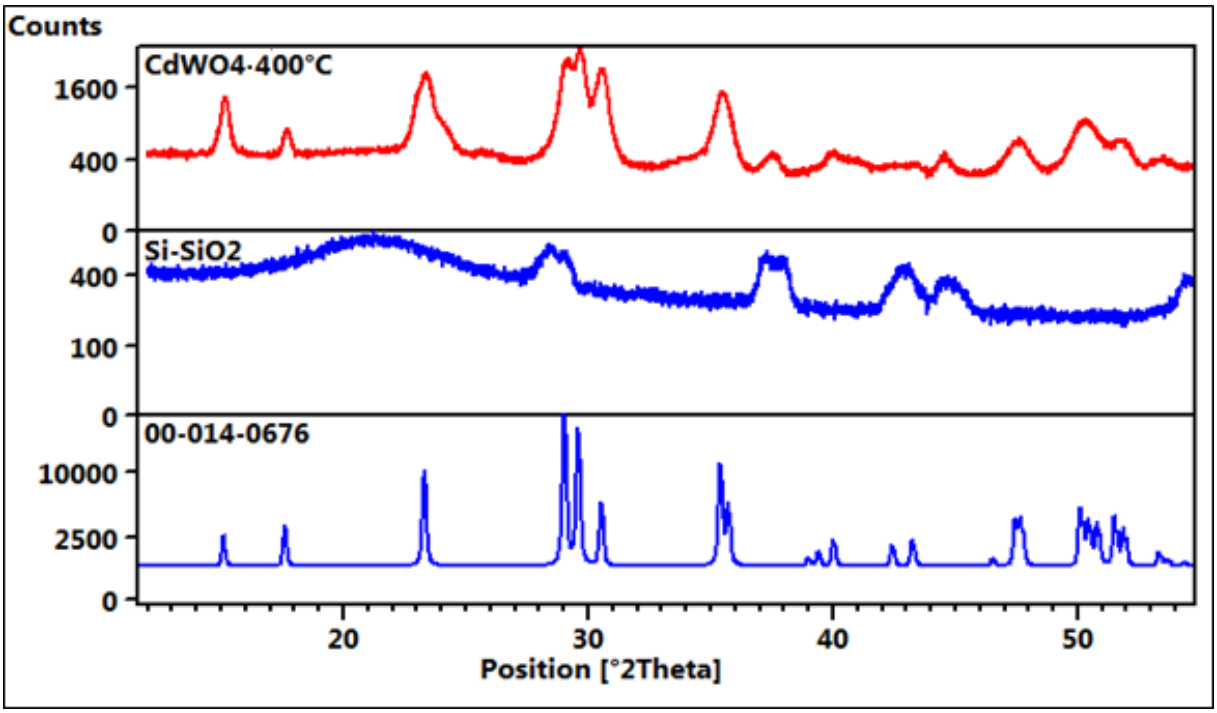
Counts
CdWO4·400°C
1600
400
0
Si-SiO2
400
100
0
00-014-0676
10000
2500
0
20
30
40
50
Position [°2Theta]

Fig. 2b:

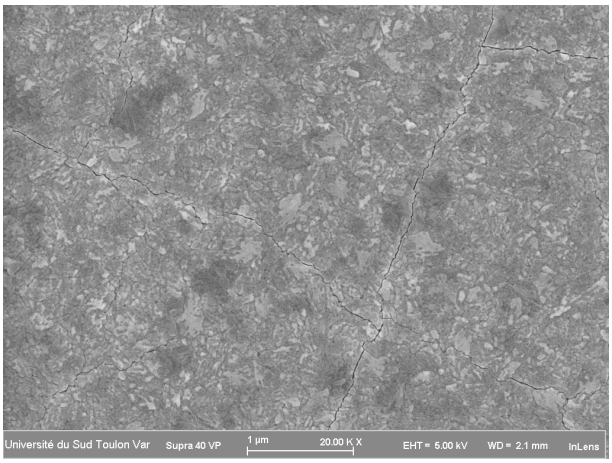
Université du Sud Toulon Var Supra 40 VP 1 µm 20.00 K X EHT = 5.00 kV WD = 2.1 mm InLens

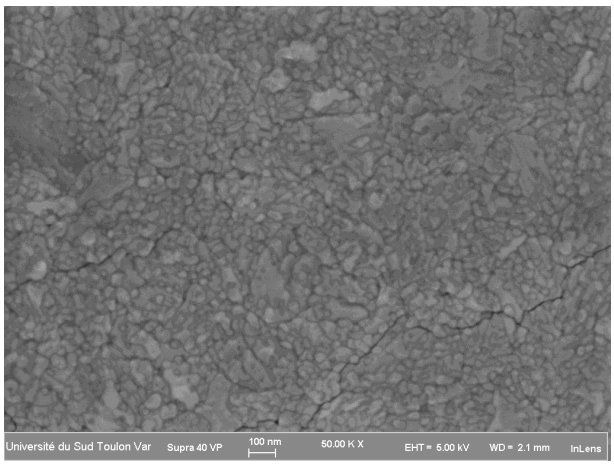
Université du Sud Toulon Var Supra 40 VP 100 nm 50.00 K X EHT = 5.00 kV WD = 2.1 mm InLens

Fig. 3a:

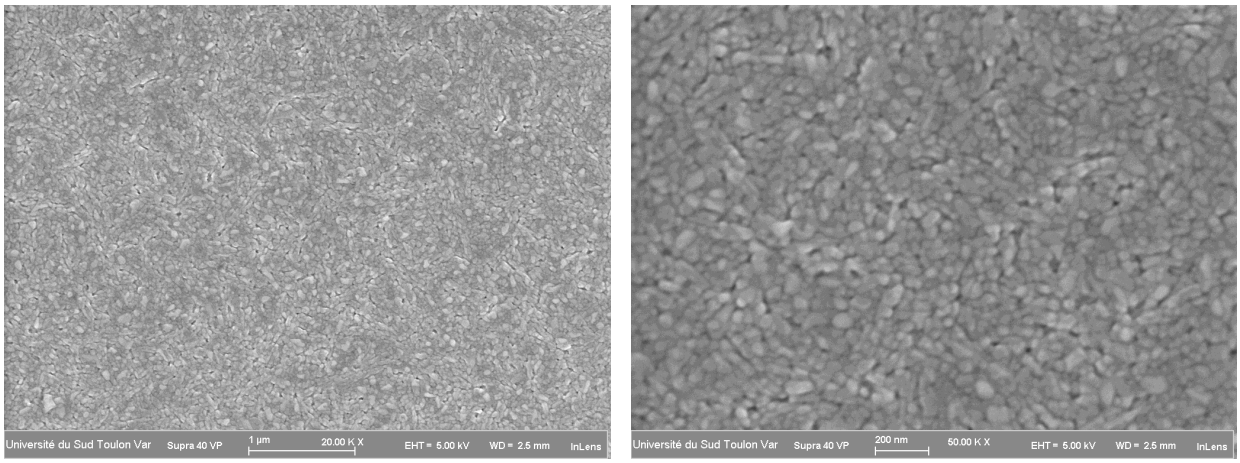
Université du Sud Toulon Var Supra 40 VP 1 µm 20.00 K X EHT = 5.00 kV WD = 2.5 mm InLens
Université du Sud Toulon Var Supra 40 VP 200 nm 50.00 K X EHT = 5.00 kV WD = 2.5 mm InLens

Fig. 3b:

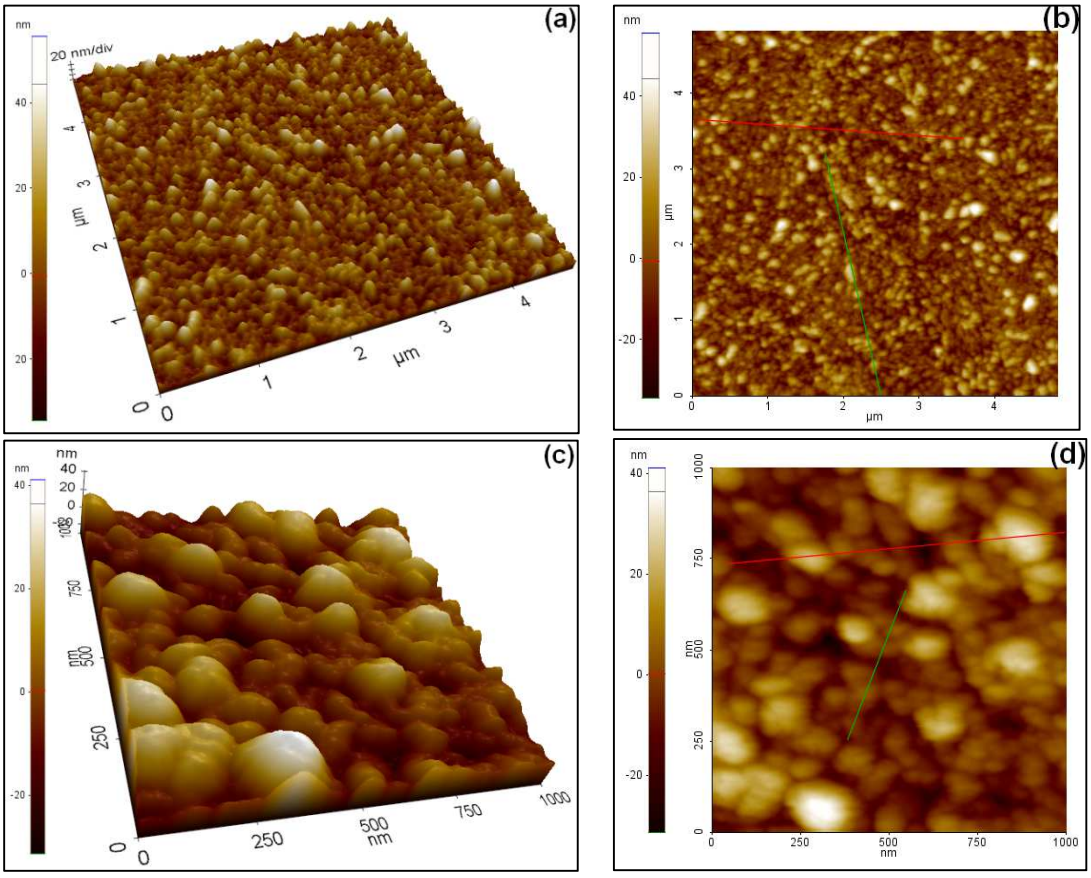
(a)
nm
20 nm/div
μm
(b)
nm
μm
(c)
nm
nm
(d)
nm
nm

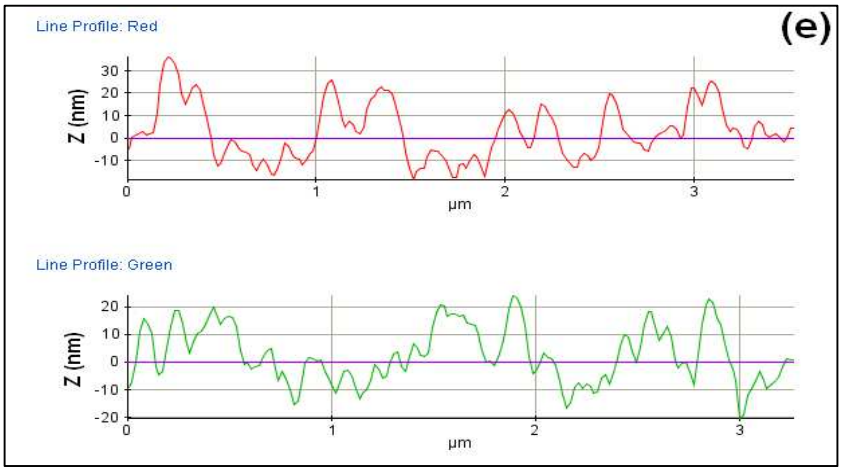
(e)
Line Profile: Red
Z (nm)
μm
Line Profile: Green
Z (nm)
μm

Fig. 4abcde:

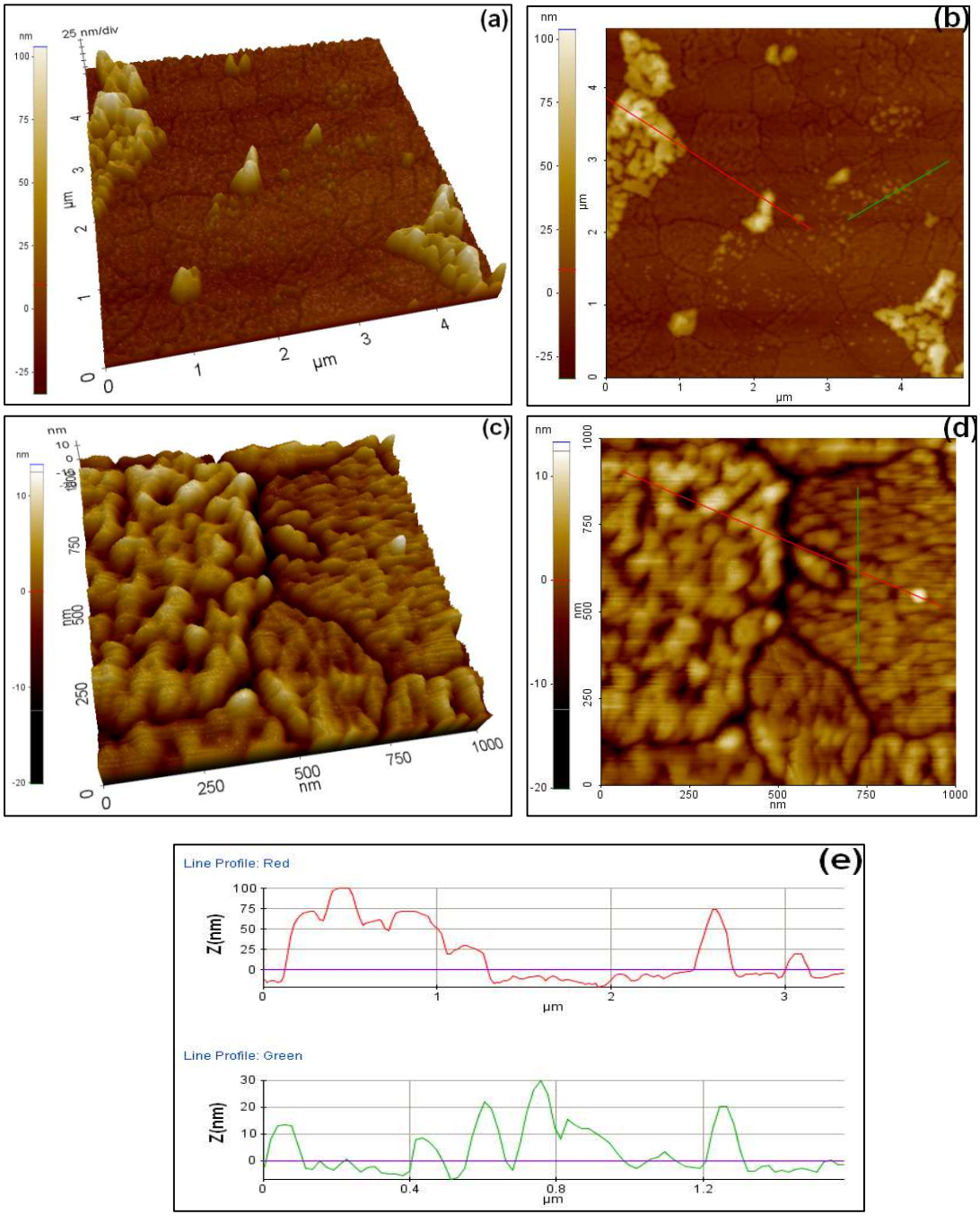
(a)
25 nm/div
nm
µm
(b)
nm
µm
(c)
nm
nm
(d)
nm
nm
(e)
Line Profile: Red
Z(nm)
µm
Line Profile: Green
Z(nm)
µm

Fig. 5abcde:

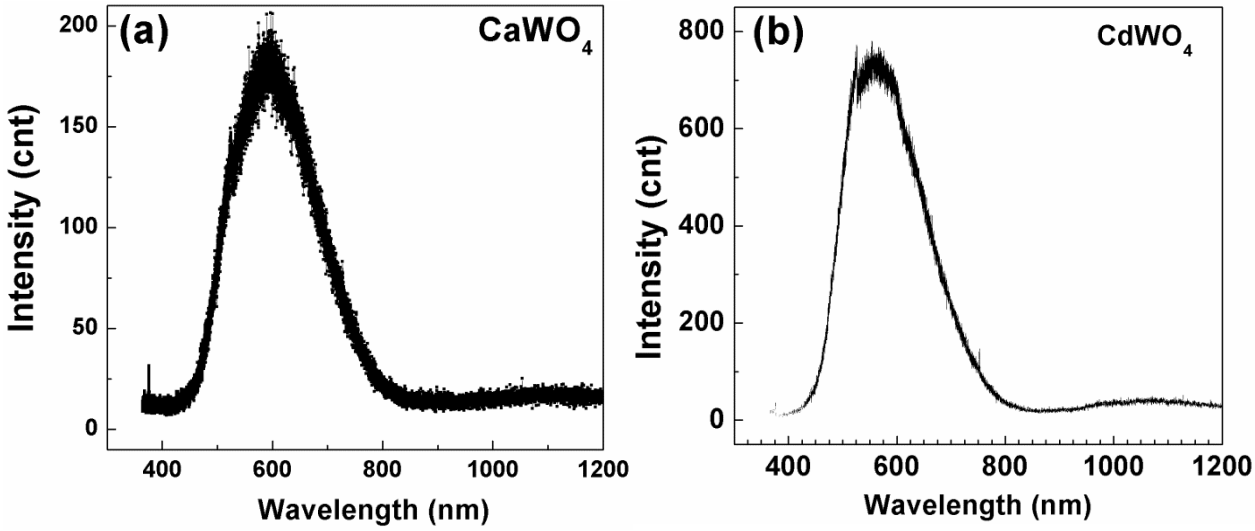

Fig. 6a, b:

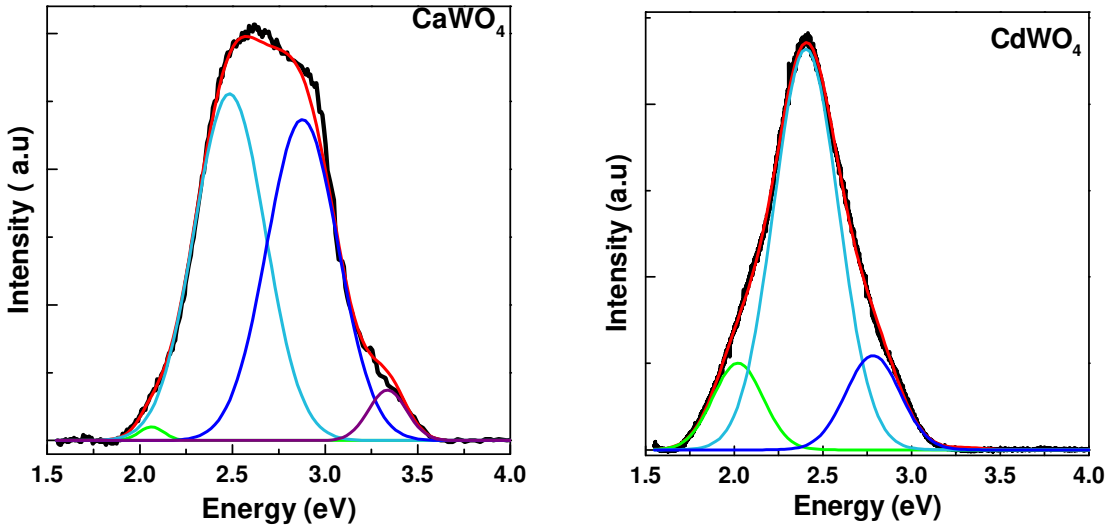
CaWO4
Intensity (a.u)
1.5
2.0
2.5
3.0
3.5
4.0
Energy (eV)
CdWO4
Intensity (a.u)
1.5
2.0
2.5
3.0
3.5
4.0
Energy (eV)

Figure 6c,d:

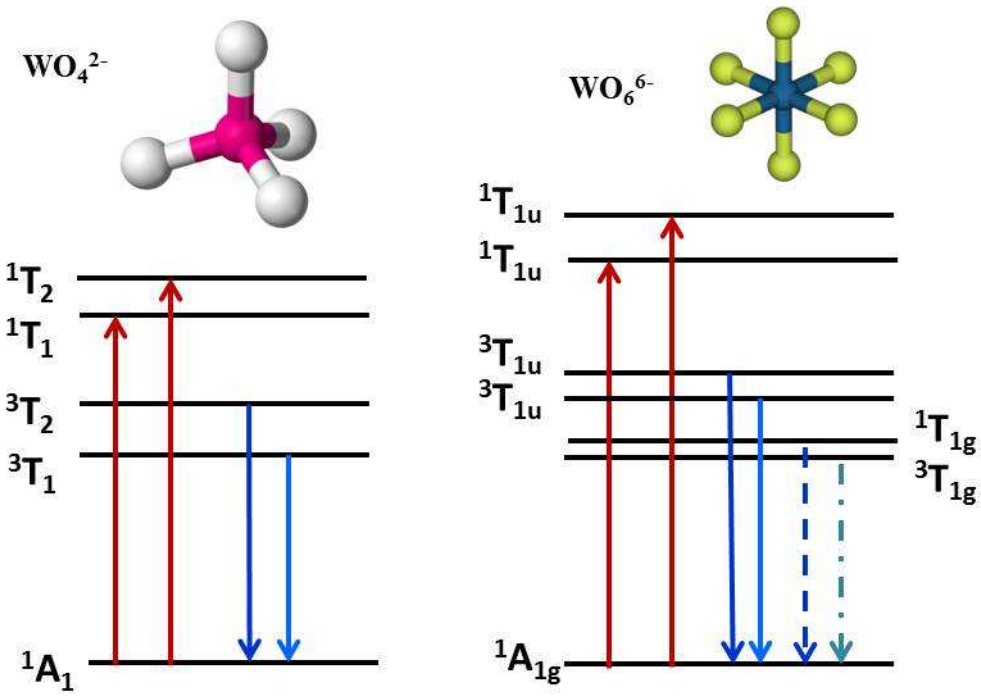
WO4 2-
WO6 6-
1T2
1T1
3T2
3T1
1A1
1T1u
1T1u
3T1u
3T1u
1T1g
3T1g
1A1g

Fig. 7:

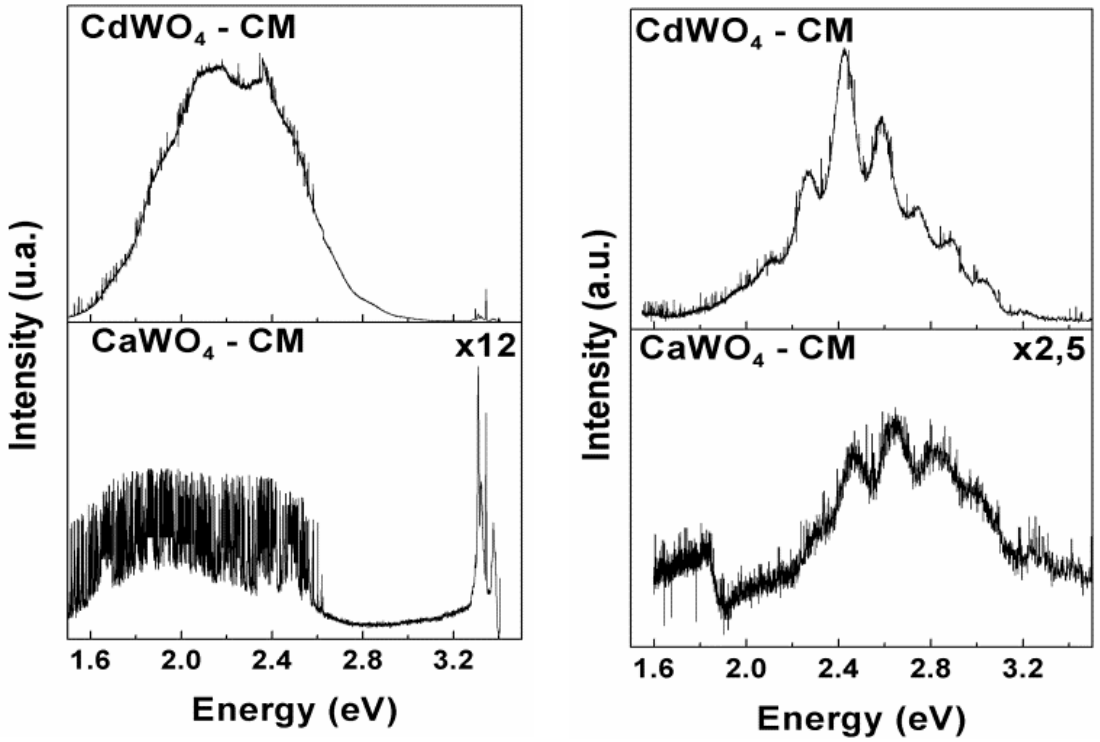
CdWO4 - CM
CaWO4 - CM
x12
Intensity (u.a.)
1.6
2.0
2.4
2.8
3.2
Energy (eV)
CdWO4 - CM
CaWO4 - CM
x2,5
Intensity (a.u.)
1.6
2.0
2.4
2.8
3.2
Energy (eV)

Fig. 8:

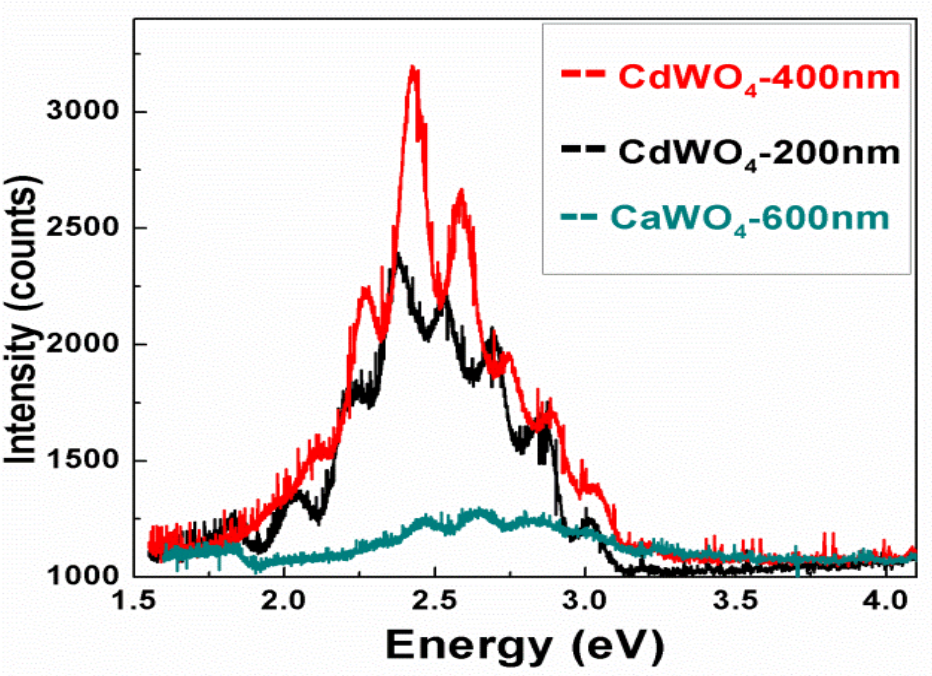
CdWO4-400nm
CdWO4-200nm
CaWO4-600nm
Intensity (counts)
3000
2500
2000
1500
1000
1.5
2.0
2.5
3.0
3.5
4.0
Energy (eV)

Fig. 9:

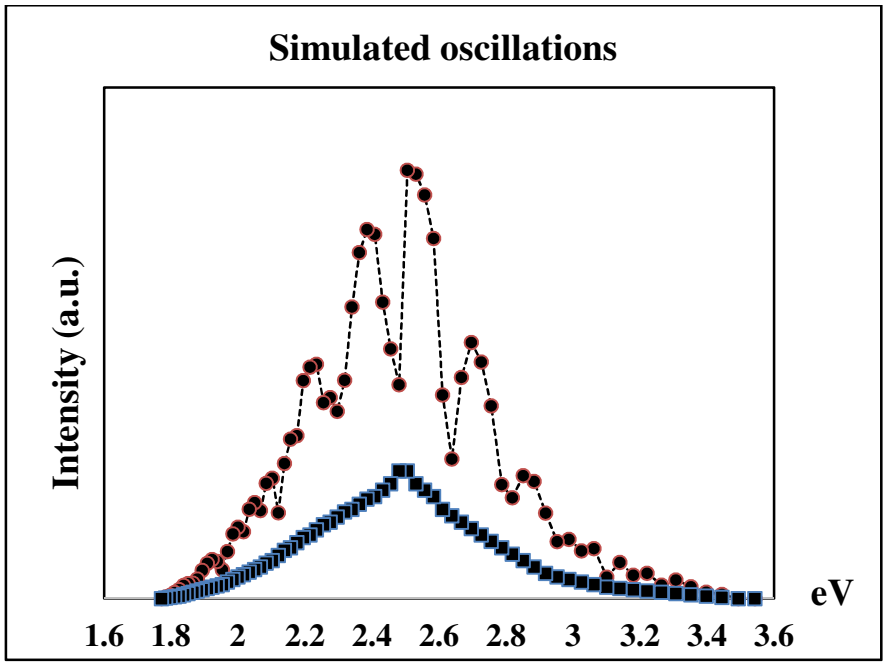
Simulated oscillations
Intensity (a.u.)
eV
1.6
1.8
2
2.2
2.4
2.6
2.8
3
3.2
3.4
3.6

Fig. 10:

Table 1:

	$CdWO_4$ (200 nm)	**$CdWO_4$ (400 nm)**	**$CaWO_4$ (600 nm)**
Gas	Ar : O_2 (90 : 10)	Ar : O_2 (90 : 10)	Ar : O_2 (90 : 10)
Vaccum Pressure (mbar)	5.10^{-6}	5.10^{-6}	6.510^{-6}
Ar flow (sccm)	27	27	27
O_2 flow (sccm)	3	3	3
Ar pressure (mbar)	14.10^{-3}	14.10^{-3}	14.10^{-3}
Power (W)	25	25	50
Target tension (V)	20	20	100
Deposit time (h)	3	5	2

Table 2:

	$CdWO_4$ (200 nm) Monoclinic	**$CdWO_4$ (400 nm)** Monoclinic	**$CaWO_4$ (600 nm)** Tetragonal
a (σ_a) (10^{-10}m)	5.01 (0.02)	5.02 (0.02)	5.21 (0.02)
b (σ_b) (10^{-10}m)	5.81 (0.01)	5.83 (0.01)	5.21 (0.02)
c (σ_c) (10^{-10}m)	5.05 (0.02)	5.06 (0.02)	11.33 (0.01)
β (σ_β) (°)	91.32 (0.02)	91.34 (0.02)	90

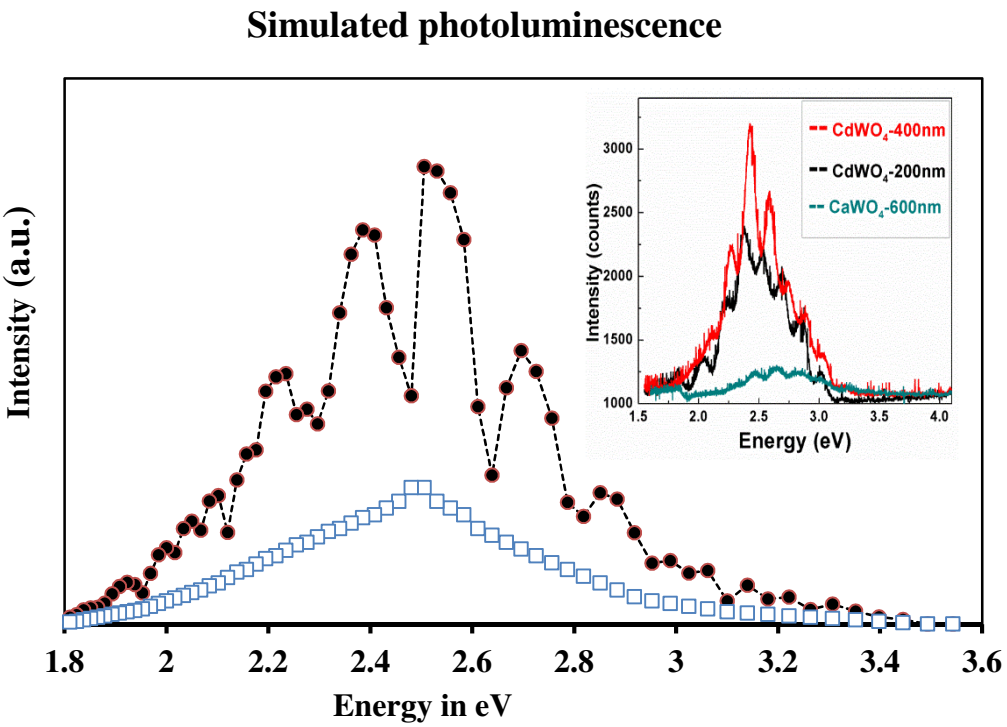
Simulated photoluminescence
Intensity (a.u.)
1.8
2
2.2
2.4
2.6
2.8
3
3.2
3.4
3.6
Energy in eV
CdWO4-400nm
CdWO4-200nm
CaWO4-600nm
Intensity (counts)
3000
2500
2000
1500
1000
1.5
2.0
2.5
3.0
3.5
4.0
Energy (eV)